Delft University of Technology

Stability of Guided Parachute-Payload Systems for Planetary Descent

Trovarelli, Federico; Mooij, Erwin

DOI
10.2514/6.2019-0665

Publication date
2019

Document Version
Final published version

Published in
AIAA Scitech 2019 Forum

Citation (APA)
Trovarelli, F., & Mooij, E. (2019). Stability of Guided Parachute-Payload Systems for Planetary Descent. In *AIAA Scitech 2019 Forum: 7-11 January 2019, San Diego, California, USA* Article AIAA 2019-0665 https://doi.org/10.2514/6.2019-0665

Important note
To cite this publication, please use the final published version (if applicable).
Please check the document version above.

Copyright
Other than for strictly personal use, it is not permitted to download, forward or distribute the text or part of it, without the consent of the author(s) and/or copyright holder(s), unless the work is under an open content license such as Creative Commons.

Takedown policy
Please contact us and provide details if you believe this document breaches copyrights.
We will remove access to the work immediately and investigate your claim.

This work is downloaded from Delft University of Technology.
For technical reasons the number of authors shown on this cover page is limited to a maximum of 10.

AIAA SciTech Forum
7-11 January 2019, San Diego, California
AIAA Scitech 2019 Forum

10.2514/6.2019-0665

Check for updates

Stability of Guided Parachute-Payload Systems for Planetary Descent

Federico Trovarelli* and Erwin Mooij†
Delft University of Technology, Faculty of Aerospace Engineering,
Kluyverweg 1, 2629 HS Delft, The Netherlands

A key requirement for enabling manned Mars missions is the capability to land a payload within 100 m from its nominal target. State of the art technology, however, is still far from reaching this objective. A possible solution for improving the landing accuracy on Mars is the development of a guidance system that exploits thrusters installed on the backshell of the descent vehicle to control its position during the parachute descent. The research summarised here aims at evaluating how the introduction of the guidance system influences the stability properties of the parachute-payload spacecraft and what performance the resulting closed-loop system can achieve. To do this, first the dynamics of the vehicle, modelled as a rigid body, has been investigated analytically and then its response to different external perturbations was simulated by means of a multibody model. The results are encouraging and prove that the parachute descent guidance system could efficiently contribute to improving the landing accuracy on Mars.

Downloaded by TU DELFT on May 28, 2019 | http://arc.aiaa.org | DOI: 10.2514/6.2019-0665

Nomenclature

A	=	Jacobian matrix element, [varies]
$\mathbf{A}$	=	Jacobian matrix, [varies]
$\mathbf{A}$	=	State matrix, [varies]
$\mathbf{B}$	=	Input matrix, [varies]
d	=	Nominal length, [m]
C_D	=	Drag coefficient, [-]
C_L	=	Lift coefficient, [-]
C_m	=	Pitch moment coefficient, [-]
D	=	Drag force, [N]
f	=	Function, [varies]
$\mathbf{f}$	=	Multidimensional function, [varies]
g	=	Gravitational acceleration, $[\mathrm{m/s^2}]$
$\mathbf{g}$	=	Gravitational acceleration vector, $[\mathrm{m/s^2}]$
I	=	Moment of inertia, $[\mathrm{kgm^2}]$
$\mathbf{I}$	=	Inertia tensor, $[\mathrm{kgm^2}]$
$\mathbf{K}$	=	Gain matrix, [varies]
K_d	=	Derivative controller gain, [Ns/m]
K_p	=	Proportional controller gain, [N/m]
L	=	Lift force, [N]

*M.Sc. student, Section of Astrodynamics and Space Missions, f.trovarelli.1@research.gla.ac.uk. Currently: Ph.D. Candidate, University of Glasgow, School of Engineering, Glasgow, UK
†Assistant Professor, Faculty of Aerospace Engineering, e.mooij@tudelft.nl, Associate fellow AIAA

Copyright © 2019 by F. Trovarelli and E. Mooij. Published by the American Institute of Aeronautics and Astronautics, Inc., with permission.

m	=	Mass, [kg]
M	=	Moment, [Nm]
$\mathbf{M}$	=	Moment vector, [Nm]
p	=	Parachute porosity, [-]
p	=	Pressure, $\left[\mathrm{N/m^2}\right]$
P	=	Period, [s]
$\mathbf{r}$	=	Position vector, [m]
S_{ref}	=	Reference surface, $\left[\mathrm{m^2}\right]$
t	=	Time, [s]
T	=	Temperature, [K]
T	=	Thrust, [N]
$\mathbf{T}$	=	Thrust vector, [N]
$\mathbf{u}$	=	Control vector, [varies]
$\mathbf{x}$	=	State vector, [varies]
α	=	Angle of attack, [rad]
γ	=	Flight-path angle, [rad]
Δ_{h_t}	=	Gust transient size, [m]
ζ	=	Damping factor, [-]
θ	=	Attitude angle, [deg]
λ	=	Eigenvalue, [varies]
ρ	=	Atmospheric density, $\left[\mathrm{kg/m^3}\right]$
ω_n	=	Natural frequency, [Hz]

I. Introduction

The first soft landing on the Red Planet, after many failed attempts, dates back to 19 June 1976 when the NASA lander Viking touched down in Chryse Planitia. Viking was followed by Mars Pathfinder (MPF) and Mars Exploration Rover (MER), in which new landing concepts were tested. All these missions were not designed for achieving high landing accuracy at touchdown. After the first Mars missions, however, the objective of landing the first man on Mars as well as new scientific needs triggered the development of new technologies to ensure the capability to deliver a large cargo close to a previously landed asset or in a specific spot within a hazardous Martian region. For responding to this need, NASA addressed the so-called *pinpoint landing accuracy requirement*, requesting that a payload can be landed within 100 m from its desired target. The first effort in this direction is represented by the launch of the Mars Science Laboratory (MSL) mission in 2011. In fact, thanks to the implementation of an autonomous guidance and control system for the hypersonic entry phase the 900 kg rover Curiosity could be delivered inside a 10-km landing ellipse.

Even if MSL represented a significant advancement in Mars entry, descent and landing (EDL) technology, pinpoint landing accuracy is still far from being reached. The residual dispersion is due to a number of sources. Amongst these, the navigation error is the most relevant and affects, with variable magnitude, all the phases of the classical Viking-derived EDL sequence, i.e., the entry, parachute flight and powered terminal descent. A second source of dispersion are the unpredictable winds that cause the spacecraft to drift away from its nominal trajectory during the parachute descent. This flight phase, after MSL, remains the only EDL mission segment during which the spacecraft is not guided. A system that can control the trajectory of the vehicle during the parachute flight could compensate for the wind drift effect and contribute to the size reduction of the landing ellipse on the surface of Mars.[1]

Considering these, the present study will first determine how a guidance system that exploits the thrust produced by hydrazine thrusters installed on the backshell of the system for controlling its trajectory during the parachute phase, influences the dynamic stability properties of the spacecraft, fundamental for mission success. This requires that the characteristic behaviour of the system is analysed for both the open-loop and closed-loop cases and then compared. Second, the performance that the parachute descent guidance system can achieve will be defined by means of a simulation approach and subsequently discussed.

Downloaded by TU DELFT on May 28, 2019 | http://arc.aiaa.org | DOI: 10.2514/6.2019-0665

The layout of this paper is as follows. In Sec. II the reference mission and vehicle are introduced, as well as the different employed parachute models. Verification and validation of the developed system is discussed in Sec. III. The results are given in two sections, i.e, Sec. IV presents the rigid-body stability analysis, whereas Sec. V focusses on the multibody system performance. Section VI, finally, concludes the paper with some final remarks.

II. Modelling

For studying the characteristic behaviour and the stability properties of a parachute-payload vehicle, a model that can reproduce its dynamic is needed. Some pioneering studies focusing on the stability of these systems, such as Refs. 2, 3 and 4, exploit models that are normally derived using either Newton or Lagrange mechanics. These models are characterised by a low number of degrees of freedom (DOF) and offer a better insight into the physics of the problem.

When higher fidelity is required, however, and the number of interconnected bodies and DOF of the system increase, then the task of determining the equations of motion (EOM) using either Newton or Lagrange methods increases accordingly. Because of this, in the last decades new procedures for handling the dynamics of complex mechanical systems have been developed. By applying a multibody formalism, the user is no more concerned with the constraint forces, as with the Newton method, nor with the definition of an expression for the energy associated with the system, as happens when dealing with Lagrangian mechanics. Generally, one only has to deal with matrices that define the configuration of the multibody and force vectors. The EOM for the system are obtained automatically by manipulating these elements. Some examples of parachute-payload multibody models characterised by a large number of DOF include Refs. 5 through 8.

In the following we will use both a single rigid body and a multibody model of the reference vehicle MPF for exploiting the advantages that each of these approaches offers with respect to the analysis of the dynamic stability properties of the system. The rigid body model will indeed be used for deriving analytical results and understand how the key system parameters characterise the dynamics of the spacecraft. This model will be realised by applying the Newton approach for which an accurate investigation of the equilibrium of the forces and moments acting on the body is required. For designing the multibody model, which will be used for studying the relative motion of the elements of the parachute-payload vehicle, the approach of Neustadt[9] will be exploited.

A. Reference Mission and Vehicle

The reference mission for this study is a classical Mars EDL mission consisting of an entry phase, a parachute phase and a powered terminal-descent phase, at the end of which the lander touches down on Mars. Derived from the Viking mission scenario, this mission layout has proven to be robust, with minor variations in the parachute deployment altitude and touchdown and entry strategies. In particular, we focus our attention on the parachute descent phase. The mission data of MSL, derived from the detailed reconstruction of Ref. 10, will be used for the analysis. The nominal flight condition is assumed to be a vertical descent flight without winds, starting at 6000 m with a velocity of 100 m/s during which the spacecraft is oriented vertically. The parachute descent phase ends when the spacecraft reaches an altitude of 1000 m. Here, the residual vertical velocity is around 70 m/s and the terminal descent thrusters are supposed to ignite.

As already mentioned, the chosen reference vehicle is the MPF spacecraft. The three-body architecture of this vehicle is appropriate for housing the thrusters that in our case will be used for position control during the parachute phase. However, we decide to slightly modify its dimensions by assuming a shorter riser, 5 m instead of ≈ 20 m, between the backshell and the payload. In fact, the reasons for having such a long riser were imputable to the need of avoiding impingement of the thrusters plume with the payload and of limiting the oscillation amplitude due to gusts impacting on the vehicle at low altitudes. On the other hand, a shorter riser can result in a system that responds more quickly to commanded lateral thrust. All the mass and geometry parameters of the MPF reference vehicle are listed in Table 2.

The aerodynamic forces and moments that the parachute generates depend on the aerodynamic coefficients. Its rotational symmetry around the Z_B-axis results in the fact that its aerodynamic properties are fully defined by only three coefficients, i.e., the drag coefficient C_D, the lift coefficient C_L, and the pitch-moment coefficient C_m that are a function of the Mach number, M, and of the angle of attack, α. The aerodynamic data for the MPF disk-gap-band parachute are taken from Ref. 11, where the functions $C_D(\alpha)$,

Downloaded by TU DELFT on May 28, 2019 | http://arc.aiaa.org | DOI: 10.2514/6.2019-0665

Table 2. Mars Pathfinder spacecraft mass and geometry characteristics.[5]

Nomenclature	Description	Value
D_0 [m]	Nominal parachute diameter	12.74
S_{ref} [m^2]	Reference canopy area	127.48
p_{can} [-]	Canopy porosity	0.2
ρ_{can} [kg/m^2]	Canopy surface density	0.054
R_{can} [m]	Canopy radius	6.37
L_{sus} [m]	Suspension lines length	21.65
ρ_{sus} [kg/m^3]	Suspension lines density	1470.0
d_{sus} [m]	Suspension lines diameter	0.0015
N_{sus} [-]	Suspension lines number	40
Φ_{sus} [°]	Suspension line half-cone angle	17.37
m_{sus} [kg]	Suspension lines mass	2.3
m_{can} [kg]	Canopy mass	13.8
m_{pc} [kg]	Parachute mass	16.1
I_{pc,X_B} [kg m^2]	Moment of inertia around the X_{pc}-axis	276.16
m_{wall} [kg]	Backshell wall mass	56.9
m_{plate} [kg]	Backshell upper plate mass	2.9
m_{bs} [kg]	Backshell mass	59.8
I_{bs,X_B} [kg m^2]	Moment of inertia around the X_{bs}-axis	28.7
R_{pl} [m]	Payload radius	2
m_{pl} [kg]	Payload mass	287.8
ρ_{pl} [kg/m^3]	Payload density	8.59
I_{pl,X_B} [kg m^2]	Moment of inertia around the X_{pl}-axis	460.48
$D_{\text{pc-bs}}$ [m]	Parachute-backshell COM distance	20.66
$D_{\text{bs-pl}}$ [m]	Backshell-payload COM distance	5

$C_L(\alpha)$ and $C_m(\alpha)$ for $M = 0.29$ are determined experimentally. It has been verified that in steady-state descent the Mach number that the MPF parachute experiences is between 0.2 and 0.3. Since this condition is realistic for the the nominal steady-state flight of MPF then the values from Ref. 11 are appropriate for the purpose of the present study. The aerodynamic coefficients as a function of α are given in Fig. 1.

For modelling the added mass effect, which is a typical feature of parachute systems, one of the most straightforward approaches consists of considering it as the inertial air mass inside a hemispherical canopy:

$$m_a = \frac{2}{3}\pi \left(\frac{D_0}{2}\right)^3 \rho k_a \tag{1}$$

in which ρ is the air density and k_a is a factor that depends on the porosity of the parachute p that is generally around 0.2:

$$k_a = 1.068\left(1 - 1.465p - 0.25975p^2 + 1.2626p^3\right) \tag{2}$$

The hemispherical air mass inside the canopy also causes an increase in the inertial moment of inertia of the system. Assuming that the center of mass (COM) of the air mass coincides with the COM of the parachute, with respect to the X_B-axis then we have:

$$I_{a,X_B} = \frac{2}{5} m_a \left(\frac{D_0}{2}\right)^2 + m_a z_{\text{pc}}^2 \tag{3}$$

Since ρ is a function of altitude, the influence of added mass will vary along the descent trajectory.

Downloaded by TU DELFT on May 28, 2019 | http://arc.aiaa.org | DOI: 10.2514/6.2019-0665

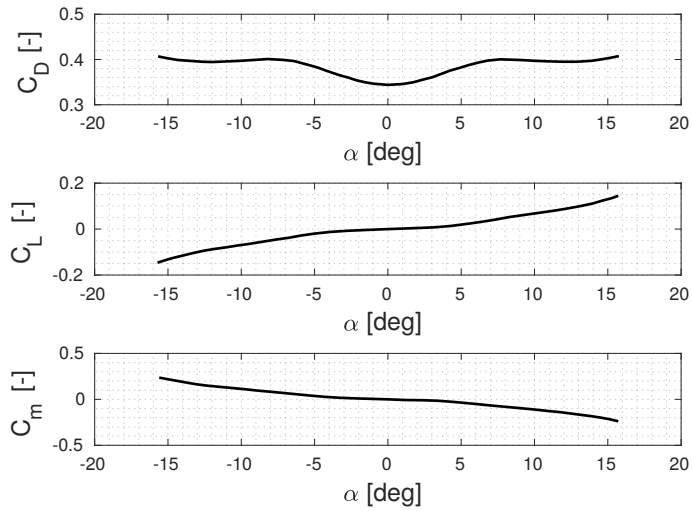

Figure 1. Mars Pathfinder parachute aerodynamic coefficients for $M = 0.29$ as a function of α. Adapted from Ref. 11.

B. Rigid Body Dynamics

The first step in the derivation of the rigid body model EOM for the parachute-payload system is the introduction of some consistent assumptions that are in agreement with the characteristics of the problem and the requirements for the analysis. The attitude motion of a parachute-payload system is characterised by two peculiar modes. The first is the pendulum-like mode while the second is the scissors-like mode. To start with the analysis of parachute-payload dynamics we only focus on the pendulum mode that can be fully described using a rigid-body model. With this approach the EOM of the model greatly simplify but, on the other hand, the information about the relative motion of the elements of the spacecraft and, in turn, about the scissors motion mode that it determines, are lost.

Second, it is assumed that all the bodies of the spacecraft, i.e., the parachute, the backshell and the payload, are rotationally symmetric and are aligned in such a way that the resulting rigid body spacecraft is rotationally symmetric as well around the Z_B-axis, as Fig. 2 shows. This configuration guarantees that the characteristics of the motion of the body around the X_B- and Y_B-axes, and along the X_I- and Y_I-axes, are analogous. In addition, the rotation about the symmetry axis Z_B does not have a significant impact on the trajectory of the spacecraft and is for now neglected. The resulting 2D 3DOF model, describing the translation along the Y_I- and Z_I-axes and the rotation around the X_B-axis, is sufficient for determining the critical information with respect to the dynamic stability of the system. Because of its simplicity, this model is appropriate to be used for analytical considerations.

The aerodynamic forces that the elements of the MPF reference spacecraft generate do not have the same magnitude and the relevance of their effect on the dynamics of the vehicle is not the same. In particular, it has been verified that the aerodynamic contribution of the parachute is one order of magnitude larger than those of the backshell or payload. Also, the aerodynamic forces generated by the parachute have a much longer lever arm with respect to those of the other elements. In fact, the COM of the whole system is closer to the most massive body that is the payload. Because of this, it is considered acceptable to neglect the aerodynamic forces and moments of the backshell and payload elements.

The translational EOM of the spacecraft, derived in agreement with these assumptions, are:

$$\mathbf{a}_I = \begin{pmatrix} \ddot{y} \\ \ddot{z} \end{pmatrix} = \begin{pmatrix} \frac{-L\sin\gamma - D\cos\gamma}{m_g} \\ g + \frac{L\cos\gamma - D\sin\gamma}{m_g} \end{pmatrix} \tag{4}$$

where the gravitational acceleration g, that pulls the spacecraft towards the surface of the planet, is negative in the inertial frame I. It is remarked that the rotation of Mars is neglected. This is justified by the fact that it is not significant for the stability properties of the dynamic system under consideration. Also, the

Downloaded by TU DELFT on May 28, 2019 | http://arc.aiaa.org | DOI: 10.2514/6.2019-0665

Downloaded by TU DELFT on May 28, 2019 | http://arc.aiaa.org | DOI: 10.2514/6.2019-0665

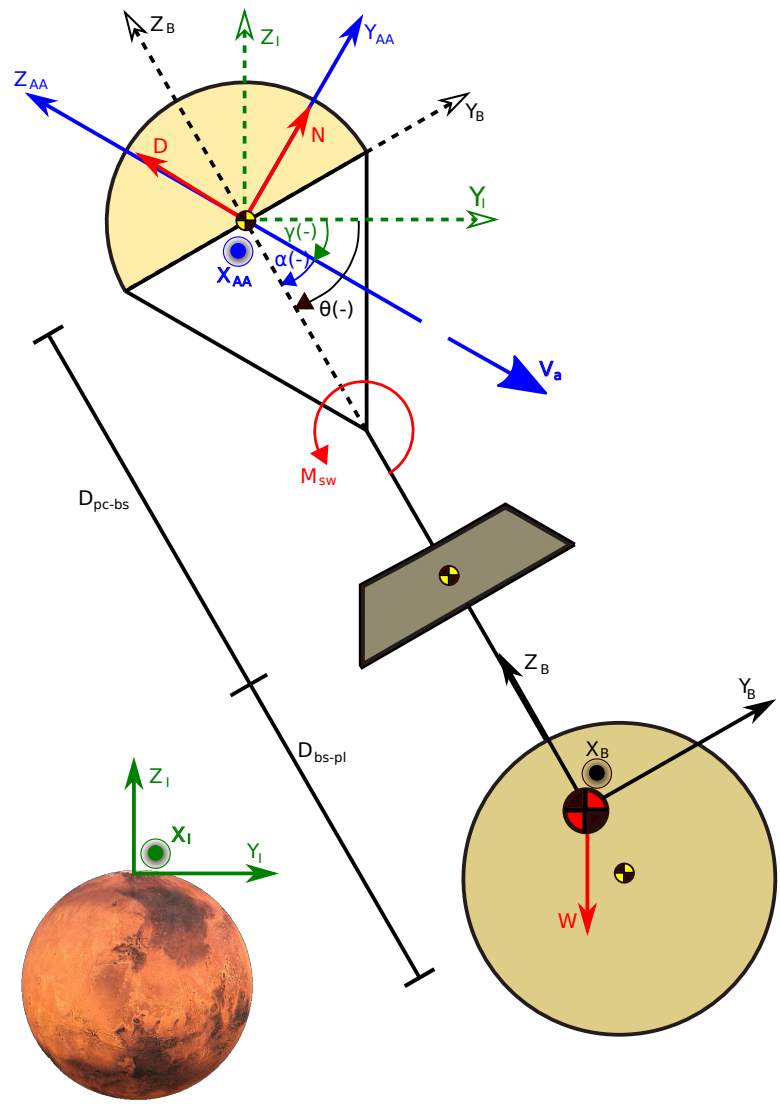

Figure 2. Parachute-backshell-payload spacecraft rigid body model dynamic analysis (dashed frames show the angle convention).

parachute flight is so short that considering the rotation of Mars does not add any level of accuracy to the subsequent analysis. Because of this, the inertial frame I is fixed to an arbitrary point on the surface of the planet. For the rotational equilibrium around the X_B-axis, if the (small) effect of the gravity gradient torque is ignored, we have:

$$\ddot{\boldsymbol{\theta}} = \frac{M_{\text{sw}} - z_{\text{COP}}(L\cos\alpha + D\sin\alpha)}{I_{X_B}}\hat{\mathbf{x}}_B \tag{5}$$

where M_{sw} is the moment around the swivel point, z_{COP} is the vertical coordinate of the centre of pressure of the parachute and I_{X_B} is the moment of inertia of the whole rigid body around the X_B-axis.

C. Multibody Dynamics

As for the rigid body model, also the multibody model will exclusively reproduce the motion of the spacecraft in a single plane perpendicular to the surface of Mars. In fact, to study dynamic stability the rotational symmetry of the system allows to introduce this simplification without loss of relevant information. The model, built using the Neustadt approach mentioned earlier, will be planar and, considering that the rotation

about the symmetry axis is neglected and that the modelling method does not imply a reduction of DOF for the multibody system, it will feature 9 DOF, two translations and one rotation per body.

The aerodynamics of the backshell and payload are also in this case neglected. In fact, the weight of the payload and the aerodynamic forces of the parachute dominate the dynamics of each single body element. This is because even if they do not act directly on a certain element, they are transmitted through the risers and are present in the dynamics of that element in the form of elastic forces.

The risers, connecting the parachute with the backshell and the backshell to the payload, are each modelled as massless springs. Also, the parachute, backshell and the payload are assumed to be rigid bodies. Each of them features its own body frame B centred in the respective COM. The parachute is assigned subscript 1, the backshell subscript 2 and the payload subscript 3. For simplicity reasons, this notation will be used in the following for indicating the gravitational masses and moments of inertia around the respective X_B-axes and other parameters related to the specific elements of the spacecraft.

To write the EOM for the multibody model we can once more refer to Fig. 2. In this case, however, the dynamics of each element of the multibody system has to be considered independently. The only difference between the rigid body and multibody models consists of the fact that in the latter case each of the elements has its own state vector components y, z and θ and includes elastic forces. Considering these, the EOM in the inertial reference frame I for each of the bodies are:

$$
\begin{aligned}
\ddot{y}_1 &= \frac{-D\cos\gamma - L\sin\gamma - F_{e,a}\cos\theta_{r,a}}{m_1 + m_a} \\
\ddot{z}_1 &= \frac{gm_1 - D\sin\gamma + L\cos\gamma - F_{e,a}\sin\theta_{r,a}}{m_1 + m_a} \\
\ddot{\theta}_1 &= \frac{-D\sin\alpha z_{\mathrm{COP}} - L\cos\alpha z_{\mathrm{COP}} + M - F_{e,a}\sin(\theta_{r,a} - \theta_1) l_{1a}}{I_1 + I_a} \\
\\
\ddot{y}_2 &= \frac{F_{e,a}\cos\theta_{r,a} - F_{e,b}\cos\theta_{r,b}}{m_2} \\
\ddot{z}_2 &= \frac{gm_2 + F_{e,a}\sin\theta_{r,a} - F_{e,b}\sin\theta_{r,b}}{m_2} \\
\ddot{\theta}_2 &= \frac{-F_{e,a}\sin(\theta_{r,a} - \theta_2) l_{2a} - F_{e,b}\sin(\theta_{r,b} - \theta_2) l_{2b}}{I_2} \\
\\
\ddot{y}_3 &= \frac{F_{e,b}\cos\theta_{r,b}}{m_3} \\
\ddot{z}_3 &= \frac{gm_3 + F_{e,b}\sin\theta_{r,b}}{m_3} \\
\ddot{\theta}_3 &= \frac{-F_{e,b}\sin(\theta_{r,b} - \theta_3) l_{3b}}{I_3}
\end{aligned}
\tag{6}
$$

In these equations, $F_{e,a}$ is the magnitude of the elastic force generated by the pseudo spring between the parachute and the backshell, $F_{e,b}$ the magnitude of the elastic force generated by the pseudo spring between the backshell and the payload, $\theta_{r,a}$ and $\theta_{r,b}$ their respective attitude angles (defined with respect to the I-frame) and l_{1a}, l_{2a}, l_{2b}, l_{3b} the distances between the anchor point of the connection (a or b) on the body and the COM of the body (1, 2 or 3). The magnitude and direction of the forces generated by the pseudo springs can be determined by calculating the inertial position of the hinges at each integration step. The position vectors for the hinges a and b connecting bodies 1, 2 and 3 are:

$$
\begin{aligned}
\mathbf{h}_{1a} &= \begin{pmatrix} y_1 + l_{1a}\cos\theta_1 \\ z_1 + l_{1a}\sin\theta_1 \end{pmatrix} & \mathbf{h}_{2b} &= \begin{pmatrix} y_2 + l_{2b}\cos\theta_2 \\ z_2 + l_{2b}\sin\theta_2 \end{pmatrix} \\
\mathbf{h}_{2a} &= \begin{pmatrix} y_2 - l_{2a}\cos\theta_2 \\ z_2 - l_{2a}\sin\theta_2 \end{pmatrix} & \mathbf{h}_{3b} &= \begin{pmatrix} y_3 - l_{3b}\cos\theta_1 \\ z_3 - l_{3b}\sin\theta_1 \end{pmatrix}
\end{aligned}
\tag{7}
$$

Downloaded by TU DELFT on May 28, 2019 | http://arc.aiaa.org | DOI: 10.2514/6.2019-0665

The elongation of the elastic connections and their orientation and the resulting magnitude of the elastic forces can be found by transforming from Cartesian to polar coordinates (the function `cart2pol` is devoted to this):

$$\begin{pmatrix} \rho_a \\ \theta_{r,a} \end{pmatrix} = \texttt{cart2pol}(\mathbf{h}_{2a} - \mathbf{h}_{1a}) \qquad F_{e,a} = -k_a \left(\rho_a - L_{\text{r,pc-bs}}\right)$$
$$\begin{pmatrix} \rho_b \\ \theta_{r,b} \end{pmatrix} = \texttt{cart2pol}(\mathbf{h}_{3b} - \mathbf{h}_{2b}) \qquad F_{e,b} = -k_b \left(\rho_b - L_{\text{r,bs-pl}}\right) \tag{8}$$

in which $L_{\text{r,pc-bs}}$ and $L_{\text{r,bs-pl}}$ are the nominal lengths of the risers and k_a and k_b the corresponding pseudo springs elastic constants. While for most of the vehicle parameters in Eq. (6) it is possible to reuse the values defined for the MPF reference but some other parameters have to be defined specifically for the multibody model.

For the elastic constants of the risers the value of $k_a = k_b = 200,000$ N/m has been assumed. Also, z_{COP} is assumed to be fixed and equal to the projection of the suspension lines on the parachute rotational symmetry axis. The riser nominal lengths are set to $L_{\text{r,pc-bs}} = 0$ m and $L_{\text{r,bs-pl}} = 5$ m. Finally, the distance of the hinge of the upper riser with respect to the parachute COM also corresponds to the projection of the suspension lines on the parachute rotational symmetry axis. The COM of the backshell is instead 0.5 m distant from the upper hinge and 1 m distant from the lower hinge. The payload COM is 2 m away from its upper hinge. It is noted that, since the model is planar, the y-coordinate of the hinge positions in the respective body frames are always 0.

D. Mars Descent Environment

The temperature and density profiles of the atmosphere of Mars can be described with the model that NASA uses for preliminary studies and in particular for aerodynamics and thermodynamics simulations. It was developed according to the atmospheric data gathered by the orbiter Mars Global Surveyor in April 1996. According to this model we have:

$$\begin{aligned} p &= 0.699 - \exp(-0.00009h) \\ T &= \begin{cases} -23.4 - 0.00222h & \text{for } h > 7000 \text{ m} \\ -31 - 0.000998h & \text{for } h < 7000 \text{ m} \end{cases} \\ \rho &= \frac{p}{0.1921\,(T + 273.1)} \end{aligned} \tag{9}$$

where the altitude h is in m, the atmospheric temperature T in °C, the atmospheric pressure p in kPa and the atmospheric density ρ in $\frac{\text{kg}}{\text{m}^3}$.

To model wind gusts, we assume that this phenomenon is limited to a certain altitude band and causes a net discontinuity in the wind-speed profile. While short horizontal wind gusts are particularly dangerous for the attitude of a parachute-payload system descending vertically in the atmosphere, a vertical gust is not critical from this point of view, because the relative motion of the body elements of the spacecraft is constrained along this direction. Oblique gusts can be seen as the composition of an horizontal and a vertical gust and do not give any additional information with respect to the dynamic properties of the system. According to the available wind data from Refs. 12 and 13, the reference gust is assumed to happen between the altitudes 3900 m and 4000 m and have a speed of 20 m/s with a transient of 10 m. This short gust is particularly appropriate for flight dynamics analysis.

A straightforward approach for evaluating how the system behaves in case of turbulence consists of testing its response using sinusoidal turbulent wind speed profiles with different frequencies. A single wind speed component in the I frame will thus be defined as:

$$V_{w,I,i} = A \sin(\omega t) \tag{10}$$

where A is the amplitude of the turbulence wind speed profile and ω its frequency. These parameters depend on the characteristics of the atmosphere of Mars. According to Ref. 14 the standard deviation σ

Downloaded by TU DELFT on May 28, 2019 | http://arc.aiaa.org | DOI: 10.2514/6.2019-0665

Table 3. Descent trajectory comparison: simulation by Trovarelli *vs* data derived from Ref. 15 (IC: $\gamma_0 = -25.83°$, $\theta_0 = -25.83°$, $\dot{\theta}_0 = 0°/\mathbf{s}$, $V_0 = 386\ \frac{\mathbf{m}}{\mathbf{s}}$, $z_0 = 8600$ m, $y_0 = 0$ m).

	Spencer et al. [1996][15]		Trovarelli		$\mid \Delta\% \mid$	
h [m]	**t** [s]	$\mathbf{V}_z$ [m/s]	**t** [s]	$\mathbf{V}_z$ [m/s]	$\mid \Delta\mathbf{t}\% \mid$	$\mid \Delta\mathbf{V}_z\% \mid$
8600	0	-175.3	0	-175.3	0	0
6500	20.0	-71.7	22.4	-75.1	12.0	4.7
4700	45.0	-72.4	46.0	-77.2	2.2	6.6
1500	92.0	-65.0	89.0	-70.2	3.3	9.0
300	111.0	-62.0	106.6	-66.5	4.0	7.3
50	115.0	-60.0	110.4	-65.8	4.0	9.7

for the turbulence in the planetary boundary layer is 2.4 m/s for both the horizontal and vertical velocity components. This value can be used as amplitude A of the periodic signal. The turbulence frequency, ω, for reasons introduced earlier, is not a unique value. It varies within a frequency spectrum whose lower extreme can be derived from the smallest scale of the vortices that can be found in a turbulent flow. The maximum signal frequency of the turbulence-velocity profile, corresponding to the smaller possible size of the eddies (7 mm), is 40.82 Hz, according to the definition of turbulence from Kolmogorov. The lower extreme for the desired frequency spectra, instead, cannot be derived from physical considerations.

To model the Mars gravity field we choose to use the inverse square law. With respect to the inertial frame I fixed to Mars defined the gravitational acceleration vector can be defined as:

$$\mathbf{g}_I = \begin{pmatrix} 0 \\ 0 \\ -\frac{\mu_M}{(R_M+z)^2} \end{pmatrix} = \begin{pmatrix} 0 \\ 0 \\ g \end{pmatrix} \tag{11}$$

where z is the altitude over the surface of Mars, μ_M=4.282837×10^{13} m^3/s^2 and R_M=3389.5 km.

III. Verification and Validation

The rigid body and multibody dynamic models developed earlier have both been verified with a number of tests. In particular, the former has been tested by analysing the behaviour of the system in vacuum and its convergence to the equilibrium condition. Also, the descent trajectory of MPF simulated with this model has been compared with real MPF mission data. This test is reported below. The tests with the rigid body model are also relevant for the multibody model that directly derives from it. In addition, however, the multibody methodology applied has been tested by simulating a double pendulum and comparing the results with those obtained using a Lagrange description. Finally, the energy dissipation of the multibody model and its convergence to the equilibrium condition have also been analysed.

The parachute descent of the MPF vehicle has been simulated with the rigid body model and compared with the data from Ref. 15. The comparison is available in Table 3. The first part of the simulated trajectory, between the altitudes of 8600 m and 4700 m, corresponds to the transient phase. In here, after deployment the parachute stabilises the payload until the vertical flight condition is reached. In this case the simulated trajectory shows a delay with respect to the reference data. This delay is due to the fact that the model does not consider the inflation of the parachute. In other words, in the real case the parachute does not immediately generate the maximum drag, because it needs time to reach its nominal dimension. Also, after 4700 m the vertical velocity stabilises around its equilibrium value. In this case the situation is opposite with respect to the transient phase because the simulated spacecraft decelerates less than in the real case and stabilises on a larger vertical equilibrium velocity. This can be explained by considering that the dynamic model neglects the drag force generated by the elements other than the parachute. These would clearly contribute to further decelerating the vehicle. These considerations, together with the good correspondence of the two trajectories, confirm the success of this test.

Downloaded by TU DELFT on May 28, 2019 | http://arc.aiaa.org | DOI: 10.2514/6.2019-0665

Downloaded by TU DELFT on May 28, 2019 | http://arc.aiaa.org | DOI: 10.2514/6.2019-0665

IV. Rigid Body Stability Analysis

The stability properties of the linearised system in the vicinity of the linearisation point, under the conditions of the Indirect Method of Lyapunov, correspond to those of the nonlinear system it is derived from. Because of this, the stability properties of the nonlinear system can be determined by studying the eigenvalues of the Jacobian matrix of the linearised system. The 3DOF nonlinear system describing the parachute-payload system descending in the atmosphere of Mars introduced earlier can be linearised by introduncing in it some assumptions. First, the descent flight is assumed to take place in steady-state conditions. The linearisation point along the steady-state trajectory is:

$$\mathbf{x}_{\text{ss}} = \begin{pmatrix} y = x_1 = 0 \text{ [m]} \\ z = x_2 = 1000 \text{ [m]} \\ \theta = x_3 = 90^\circ \\ V_y = x_4 = 0 \\ V_z = x_5 = 70 \ \left[\frac{\text{m}}{\text{s}}\right] \\ \dot{\theta} = x_6 = 0 \end{pmatrix}, \quad \alpha = 0, \quad \gamma = 90^\circ \tag{12}$$

Also, the description of the aerodynamic coefficents is simplified to:

$$\begin{aligned} C_D &= C_D(0) = C_{D,0} & C_{D,0} &= 0.3449 \\ C_L &= k_{C_L}\alpha & k_{C_L} &= 0.4414 \\ C_m &= k_{C_m}\alpha & k_{C_m} &= -0.7212 \end{aligned} \tag{13}$$

By considering the gravity and atmosphere density constant (because of this the added mass effect is constant and the total body inertial mass and moment of inertia around the X_B-axis, given by m and I_{tot} respectively, are constant as well), and by neglecting the terms that have a lower magnitude in the EOM of the system, the elements of the Jacobian matrix describing the linearised system, after rearrangement, are:

$$\begin{aligned}
&\frac{\partial f_1}{\partial x_1} = 0, \quad \frac{\partial f_1}{\partial x_2} = 0, \quad \frac{\partial f_1}{\partial x_3} = 0, \quad \frac{\partial f_1}{\partial x_4} = 1, \quad \frac{\partial f_1}{\partial x_5} = 0, \quad \frac{\partial f_1}{\partial x_6} = 0; \\
&\frac{\partial f_2}{\partial x_1} = 0, \quad \frac{\partial f_2}{\partial x_2} = 0, \quad \frac{\partial f_2}{\partial x_3} = 0, \quad \frac{\partial f_2}{\partial x_4} = 0, \quad \frac{\partial f_2}{\partial x_5} = 1, \quad \frac{\partial f_2}{\partial x_6} = 0; \\
&\frac{\partial f_3}{\partial x_1} = 0, \quad \frac{\partial f_3}{\partial x_2} = 0, \quad \frac{\partial f_3}{\partial x_3} = 0, \quad \frac{\partial f_3}{\partial x_4} = 0, \quad \frac{\partial f_3}{\partial x_5} = 0, \quad \frac{\partial f_3}{\partial x_6} = 1; \\
&\frac{\partial f_4}{\partial x_1} = 0, \quad \frac{\partial f_4}{\partial x_2} = 0, \quad \frac{\partial f_4}{\partial x_3} = \frac{S_{\text{ref}}\,\rho\, {x_5}^2 k_{C_L}}{2m}, \quad \frac{\partial f_4}{\partial x_4} = \frac{S_{\text{ref}}\,\rho\, x_5\,(C_{D,0} + k_{C_L})}{2m}, \\
&\frac{\partial f_4}{\partial x_5} \approx 0, \quad \frac{\partial f_4}{\partial x_6} = -\frac{S_{\text{ref}}\,\rho\, x_5\, z_{\text{pc}}\,(C_{D,0} + k_{C_L})}{2m}; \\
&\frac{\partial f_5}{\partial x_1} = 0, \quad \frac{\partial f_5}{\partial x_2} = 0, \quad \frac{\partial f_5}{\partial x_3} = 0, \quad \frac{\partial f_5}{\partial x_4} = 0, \quad \frac{\partial f_5}{\partial x_5} = \frac{C_{D,0}\, S_{\text{ref}}\,\rho\, x_5}{m}, \quad \frac{\partial f_5}{\partial x_6} = 0; \\
&\frac{\partial f_6}{\partial x_1} = 0, \quad \frac{\partial f_6}{\partial x_2} = 0, \quad \frac{\partial f_6}{\partial x_3} = -\frac{S_{\text{ref}}\,\rho\, {x_5}^2\,(C_{D,0}\, z_{\text{pc}} - D_0\, k_{C_m} + z_{\text{pc}}\, k_{C_L})}{2I_{\text{tot}}}, \\
&\frac{\partial f_6}{\partial x_4} = -\frac{S_{\text{ref}}\,\rho\, x_5\,(C_{D,0}\, z_{\text{pc}} - k_{C_m}\, D_0 + k_{C_L}\, z_{\text{pc}})}{2I_{\text{tot}}}, \\
&\frac{\partial f_6}{\partial x_5} \approx 0, \quad \frac{\partial f_6}{\partial x_6} = \frac{S_{\text{ref}}\,\rho\, x_5\, z_{\text{pc}}\,(C_{D,0}\, z_{\text{pc}} - D_0\, k_{C_m} + z_{\text{pc}}\, k_{C_L})}{2I_{\text{tot}}};
\end{aligned} \tag{14}$$

A. Open-Loop System Stability

Analytically solving the characteristic equations for determining the eigenvalues of the full [6×6] matrix is not possible. By identifying and solving smaller blocks each related to the eigenmotions of the system, with the help of the numerically computed eigenvectors of the matrix $\mathbf{A}$, it is possible to get approximated analytical expressions for these eigenvalues. The eigenvalues related to the vertical and horizontal velocity are respectively:

$$\lambda_{V_z} = \frac{\partial f_5}{\partial x_5} = \frac{C_{D,0}\, S_{\text{ref}}\, \rho\, x_5}{m} \tag{15}$$

$$\lambda_{V_y} = \frac{S_{\text{ref}}\, \rho\, x_5}{2} \left(-\frac{\left(C_{D,0} + k_{C_L}\right) z_{\text{pc}} - k_{C_m} D_0}{I_{\text{tot}}} k_{1,o} + \frac{C_{D,0} + k_{C_L}}{m} k_{2,o} \right) \tag{16}$$

where the coefficients $k_{1,o}$ and $k_{2,o}$, determined by means of an optimization that minimises the error between the analytical and numerical eigenvalues for the MPF reference vehicle flying in steady-state conditions, are:

$$k_{1,o} = 0.047611578, \quad k_{2,o} = 0.489989999 \tag{17}$$

Finally, for the rotational eigenmotion, the complex and conjugate eigenvalues are expressed as:

$$\lambda_\theta = \frac{x_5}{2} \left(k z_{\text{pc}} \pm i \sqrt{k \left(k z_{\text{pc}}^2 - 4 \right)} \right), \quad \text{with} \quad k = \frac{S_{\text{ref}}\, \rho\, \left(C_{D,0}\, z_{\text{pc}} - D_0\, k_{C_m} + z_{\text{pc}}\, k_{C_L} \right)}{2 I_{\text{tot}}} \tag{18}$$

The analytical eigenvalues given by Eqs. (15), (16) and (18) yield accurate results for the dynamics of the MPF reference vehicle in steady-state descent. In particular, while λ_{V_z} is exact, the approximation introduced to derive λ_θ causes errors in the order of 2% for both the real and imaginary parts. Also, the introduction of the coefficients $k_{1,o}$ and $k_{2,o}$ causes an error for λ_{V_y} that is always smaller than 0.015% throughout the descent with respect to the case in which it is defined numerically. These coefficients have been determined for the MPF reference vehicle, so that if its configuration changes then the error λ_{V_y} will grow. Nevertheless, even large variations (up to ±100% with respect to MPF reference value) in vehicle mass and geometry or aerodynamic parameters, cause an additional relative error in the order of 1%. All together, this demonstrates that the analytical definition of the eigenvalues derived for the parachute-payload system is consistent and can be used for further analysis.

The first interesting aspect to notice about the dynamics of the system is that for our reference configuration λ_θ are complex and conjugate, with negative real part. This implies that the rotational eigenmotion is periodical and converges to the equilibrium point. For this eigenmotion it is possible to determine the natural frequency ω_θ, the damping factor ζ_θ and the period P_θ. After rearranging:

$$\omega_\theta = \left| x_5 \right| \sqrt{k}, \qquad \zeta_\theta = \frac{\sqrt{k} z_{\text{pc}}}{2}, \qquad P_\theta = \frac{4\pi}{\left| x_5 \right| \sqrt{k \left(k z_{\text{pc}}^2 - 4 \right)}} \tag{19}$$

These expressions confirm the physical expectations about the attitude behaviour of the parachute-payload system. It is clear that the characteristics of the pendulum motion of the system result from the balance between the inertia properties of the body and the effect of the aerodynamic forces, mathematically expressed by the parameter k. In general, a larger k, corresponding to a predominance of the aerodynamic contributions, results in higher frequency and better damped oscillations. If k is smaller the situation is opposite, but external perturbations have a lower impact on the attitude of the system.

With respect to the single parameters appearing in the expressions above, it is easy to notice that larger $C_{D,0}$, k_{C_L} and k_{C_m} coefficients all contribute to an increase of the relative weight of the aerodynamic effect. On the other hand, the interpretation of the influence of the parameters z_{pc} and D_0, the distance of the body COM from the parachute and its radius, is not straightforward. This is due to the fact that they influence both the aerodynamic and inertia properties of the system. Finally, a smaller vertical velocity x_5 and atmospheric density ρ are responsible for a lower dynamic pressure and clearly this causes the aerodynamic contribution to lose importance.

The eigenvalues λ_{V_y} and λ_{V_z} are real and negative for the considered reference case. This suggests that the vertical and horizontal velocities will simply exhibit a converging aperiodic behaviour. Also, there is a point along the trajectory in which these values are maximum and, as a result, V_z and V_y are less stable around the corresponding equilibrium positions. This maximum corresponds to the condition in which the dynamic pressure reaches a minimum. This minimum is due to the fact that the vertical velocity x_5 has reduced due to the drag dissipation but the density ρ has not yet increased significantly as a result of the lower altitude.

The balance between aerodynamic and inertia properties of the system is also visible from analysing the equations expressing the eigenvalues for the vertical and horizontal velocity. In particular, the interpretation of Eq. (15) is straightforward. Larger $C_{D,0}$ and S_{ref} and lower m result in the fact that the vertical

Downloaded by TU DELFT on May 28, 2019 | http://arc.aiaa.org | DOI: 10.2514/6.2019-0665

velocity returns faster to the equilibrium velocity after a perturbation. Equation (16) for the horizontal-velocity eigenvalue is also interesting. It is characterised by two terms. The second term, that has m in the denominator, implies a stability behaviour analogous to that of the vertical velocity. The first term is instead due to the influence of the attitude of the vehicle on its horizontal eigenmotion. This is physically consistent. In fact, differently from the case of the vertical velocity, when the horizontal velocity is perturbed, the angle of attack of the spacecraft varies. The resulting lateral aerodynamic forces cause it to align with the airspeed. This effect, however, has an opposite sign with respect to that due to the second term, and is thus destabilising for the system's horizontal velocity. This destabilisation most probably derives from the fact that when the vehicle reorientates in the direction of the airspeed, the angle of attack caused by the presence of the perturbation reduces. As a result, the magnitude of the aerodynamic forces that had grown in horizontal direction, and that are responsible for the deceleration to V_y =0 just after the perturbation, reduce as well, and convergence to the equilibrium condition is slower. Nevertheless, the fact that $k_{1,o} << k_{2,o}$ suggests that this destabilising effect has a much smaller magnitude with respect to that due to the second term.

B. Closed-Loop System Stability

At this point we introduce the control action in the dynamics of the system. In particular, the guidance system is a proportional-derivative controller that commands the magnitude of the thrust force, produced by the backshell thrusters, as a function of the horizontal position and velocity state errors. The thrusters are assumed to be fixed with respect to the backshell and push perpendicularly to its rotational symmetry axis. The EOM of the rigid body model are modified to take into account this contribution. The thrust magnitude T, corresponding to the control input u, is a function of the state error vector:

$$T = -\mathbf{K}\boldsymbol{\Delta}\mathbf{x} = -\begin{bmatrix} K_p & 0 & 0 & K_d & 0 & 0 \end{bmatrix} \begin{bmatrix} \Delta x_1 & \Delta x_2 & \Delta x_3 & \Delta x_4 & \Delta x_5 & \Delta x_6 \end{bmatrix}^T = -K_p \Delta x_1 - K_d \Delta x_4 \tag{20}$$

where Δx_i, for $i = 1, ..., 6$ indicate the displacement of the state vector elements with respect to their references. Also in this case we will determine the stability properties of the nonlinear closed-loop system by analysing the properties of the corresponding linearised system given by:

$$\dot{\mathbf{x}} = \mathbf{A}\boldsymbol{\Delta}\mathbf{x} + \mathbf{B}\mathbf{u} \tag{21}$$

in which $\mathbf{A}$ is the state matrix, analogous to that already defined for the open-loop system whose elements are given by Eq. (14), and $\mathbf{B}$ is the control matrix defined by:

$$\mathbf{B} = \frac{\partial \mathbf{f}}{\partial \mathbf{u}} = \begin{bmatrix} 0 & 0 & 0 & -\frac{\sin x_3}{m} & \frac{\cos x_3}{m} & -\frac{z_{\text{bs}}}{I_{\text{tot}}} \end{bmatrix}^T \tag{22}$$

where $\mathbf{f}$ is the nonlinear system of EOM. For determining the stability characteristics of the closed-loop system we need to determine the eigenvalues of the state matrix:

$$\mathbf{A}^* = \mathbf{A} - \mathbf{B}\mathbf{K} \tag{23}$$

where $\mathbf{K}$ is the gain matrix. this is done similarly to the open-loop case. i.e., by identifying the eigenmotion blocks with the help of the numerical eigenvectors and by rearranging the rows and columns of the state matrix. By calculating the eigenvalues of $\mathbf{A}^*$ numerically it is has been proven that the only eigenvalues that are significantly influenced by the control action are those related to its horizontal eigenmotion that is now represented by a [2×2] block. Analytical expressions for these are:

$$\begin{aligned} \text{Re}(\lambda_y) &= \frac{S_{\text{ref}}\rho x_5 \left(C_{D,0} + k_{C_L}\right) k_{1,c}}{4m} - \frac{S_{\text{ref}}\rho x_5 \left(\left(C_{D,0} + k_{C_L}\right) z_{\text{pc}} - D_0 k_{C_m}\right) k_{2,c}}{4I_{\text{tot}}} + \frac{\sin x_3 K_d k_{1,c}}{2m} \\ \text{Im}(\lambda_y) &= \sqrt{\frac{\sin x_3 K_p k_{1,c} k_{3,c}}{m} + \frac{\text{Re}^2(\lambda_y)}{16}} \end{aligned} \tag{24}$$

where the coefficients $k_{1,c}$, $k_{2,c}$ and $k_{3,c}$ have been optimised for the MPF steady-state descent reference case:

Downloaded by TU DELFT on May 28, 2019 | http://arc.aiaa.org | DOI: 10.2514/6.2019-0665

Table 4. MPF closed-loop descent system horizontal position stability characteristics in the the steady-state point $\mathbf{x_{ss}}$ (from Eq. (12)).

Property	Value
ω_y	0.0706 $\frac{\text{rad}}{\text{s}}$
ζ_y	0.906
P_y	209.4 s
t_d	23.15 s
t_r	43.40 s
t_s	57.73 s

$$k_{1,c} = 0.6734, \quad k_{2,c} = 0.0515, \quad k_{3,c} = 1.518 \tag{25}$$

Along the steady-state trajectory the error of the analytical real part of the horizontal motion eigenvalues is always lower than $\approx 2\%$, while the imaginary part can have an error up to $\approx 20\%$. The larger error are experienced in the first part of the trajectory, where the vertical velocity is really different from the value for which it was optimised. However, if the trajectory stays close to the chosen optimisation point, then the errors reduce to a maximum of 1% for the real part and 7% for the imaginary part. In this case, also significant variations of the system parameters, for example, the payload mass or the riser length, in the order of 20%, cause an increase of only some % points in these errors. This allows us to say that the translational eigenvalues definition, given by Eq. (24), is consistent and can be used for determining the stability properties of the system, in particular in the vicinity of the linearisation point for which the coefficients $k_{1,c}$, $k_{2,c}$ and $k_{3,c}$ have been optimised.

Consider now the real part of λ_y, Eq. (24), which is characterised by three terms. The first two, that express a ratio between the aerodynamic and inertia properties of the system, are analogous to those determining λ_{V_y} in Eq. (16) for the open-loop case. In particular the second term, which includes the moment of inertia of the system in the denominator, expresses the influence of the attitude equilibrium of the system on its translational motion. As before, this term is positive for the considered MPF reference configuration but also much smaller with respect to the others ($k_{2,c} << k_{1,c}$). This means that even if it is destabilising, its contribution to the horizontal eigenmotion of the spacecraft is negligible. The first term, which is negative because $x_5 < 0$, suggests that if the aerodynamic forces generated by the parachute are larger, then it will damp faster after a perturbation in its horizontal position and velocity state. The term that marks the difference with respect to the open-loop case, however, is the third. This is directly due to the presence of the control action in the dynamics of the system and is the most important contribution to $\text{Re}(\lambda_y)$. In particular, it demonstrates that a larger derivative gain K_d and a smaller mass m contribute to making the horizontal eigenmotion of the system more stable.

The imaginary part of λ_y contains two terms with interesting aspects. One, which is negative, is proportional to the gain K_p, while the other corresponds to $\frac{\text{Re}(\lambda_y)}{4}$ squared. This second term is clearly always positive and, as described earlier, is influenced by the aerodynamic and inertia properties of the system and by the derivative gain K_d. The contribution of the two terms to $\text{Im}(\lambda_y)$ is opposite. In particular, the oscillatory behaviour is present only if the eigenvalues are complex, this requiring that the first term in $\text{Im}(\lambda_y)$ is larger than the second. In this situation, according to Eq. (24), the oscillatory motion around the equilibrium position will be more relevant in the dynamics of the vehicle if K_p is larger, K_d lower and if the inertia of the system dominates over its aerodynamic properties. This is the case for the MPF reference vehicle and mission.

As for the rotation eigenmotion, it is possible to determine analytical expressions for the the natural frequency ω_y and damping ratio ζ_y of the horizontal eigenmotion of the spacecraft. However, the interpretation of the influence that the various parameters of the spacecraft have on these characteristic values is not straightforward to analyse. This is due to the fact that the analytical expressions describing them are more complicated and exhibit the same dynamic contribution in more places. Nevertheless, it is still possible to state that, in case λ_y is complex and conjugate, a larger K_p results in a higher ω_y and lower ζ_y.

Table 4 lists the properties of the horizontal eigenmotion of the MPF reference spacecraft for the chosen gains. In particular, the delay time t_d, rise time t_r and settling time t_s have been calculated starting from the

Downloaded by TU DELFT on May 28, 2019 | http://arc.aiaa.org | DOI: 10.2514/6.2019-0665

Table 5. Set of IC for the MPF reference vehicle used for gust response open-loop system simulations.

Parameter	Value	Parameter	Value	Parameter	Value
γ_{10} [deg]	-90	γ_{20} [deg]	-90	γ_{30} [deg]	-90
θ_{10} [deg]	-90	θ_{20} [deg]	-90	θ_{30} [deg]	-90
$\dot{\theta}_{10}$ [deg/s]	0	$\dot{\theta}_{20}$ [deg/s]	0	$\dot{\theta}_{30}$ [deg/s]	0
V_{10} [m/s]	100	V_{20} [m/s]	100	V_{30} [m/s]	100
z_{10} [m]	6000	z_{20} [m]	5978.83	z_{30} [m]	5970.83
y_{10} [m]	0	y_{20} [m]	0	y_{30} [m]	0

analytical eigenvalues. The tabled values show a good similarity with the t_d, t_r and t_s estimated graphically from the linear response simulations.

V. Multibody Performance Analysis

The present section is subdivided into two main parts. First, we will discuss the dynamic response of the system to isolated and continuous inputs, simulating respectively the effect of wind gusts and turbulence that excite the motion of the spacecraft. After this, the use of backshell thrusters for controlling the horizontal position of the spacecraft during the descent will be analysed from the points of view of efficiency and performance it can achieve in correcting a horizontal position error and compensating the effect of wind.

A. Open-Loop System Performance

During the descent in the atmosphere of Mars, the system can encounter wind gusts. Assuming that it is flying in steady-state conditions, vertical gusts cause an increase in the drag forces generated by the elements of the spacecraft. This additional force, however, has no arm with respect to the connection points of the elements nor with respect to their COM and thus does not generate any moment. Vertical gusts are not an issue for the attitude dynamics of the system. The situation is different in case of a horizontal gust that instead generates horizontal force contributions. These cause the system to oscillate and may be very dangerous for its attitude motion. This principle is valid in general. Because of this we will focus on studying how the system behaves in case of horizontal perturbations that are more interesting from the dynamic stability point of view. The attitude behaviour of the MPF reference spacecraft is depicted in Fig. 3 shows how the motion of its body elements are excited at the beginning of a gust and oscillate in different ways before being damped once the gust has ended. The initial conditions for the simulation are given in Table 5. The oscillation amplitude for the attitude angle of the system elements is determined by the intensity of the gust and for the considered vehicle it can reach 45° for the payload in case of a 20 m/s gust. Also, it is interesting to notice how the oscillation of the backshell is clearly the result of the superimposition of two sinusoids with different frequencies. This characteristic is due to its direct interaction with both the parachute and the payload that, through the connection forces, impose to the backshell the respective oscillatory behaviour. The same behaviour is valid also for the other two body elements, but less noticeable.

The response of the parachute-payload system to a horizontal gust depends on its attitude when the gust is met. The spacecraft horizontal and vertical velocities of the spacecraft at the moment when the gust is met also have a significant influence on the oscillatory motion that this disturbance causes. As already suggested, the intensity of the gust that the spacecraft senses depends on the difference between the horizontal velocity of the vehicle and that of the gust. In case the vertical velocity is larger, then the variation of the angle of attack due to the same gust is lower. As a result, the horizontal aerodynamic forces that the gust generates will have a lower magnitude. In other words, the system is less sensitive to the gust. Considering these, a gust at lower altitude, where the vertical velocity of the spacecraft is lower as well, is more critical and, additionally, the system has less time for damping the resulting oscillatory motion before the terminal descent thrusters are ignited.

Many system parameters concur at determining the characteristic response of the parachute-payload system. However, most of them, such as the parachute size and the payload mass, are normally constrained by many EDL mission requirements. A system characteristic that is less constrained is its configuration. In

Downloaded by TU DELFT on May 28, 2019 | http://arc.aiaa.org | DOI: 10.2514/6.2019-0665

Downloaded by TU DELFT on May 28, 2019 | http://arc.aiaa.org | DOI: 10.2514/6.2019-0665

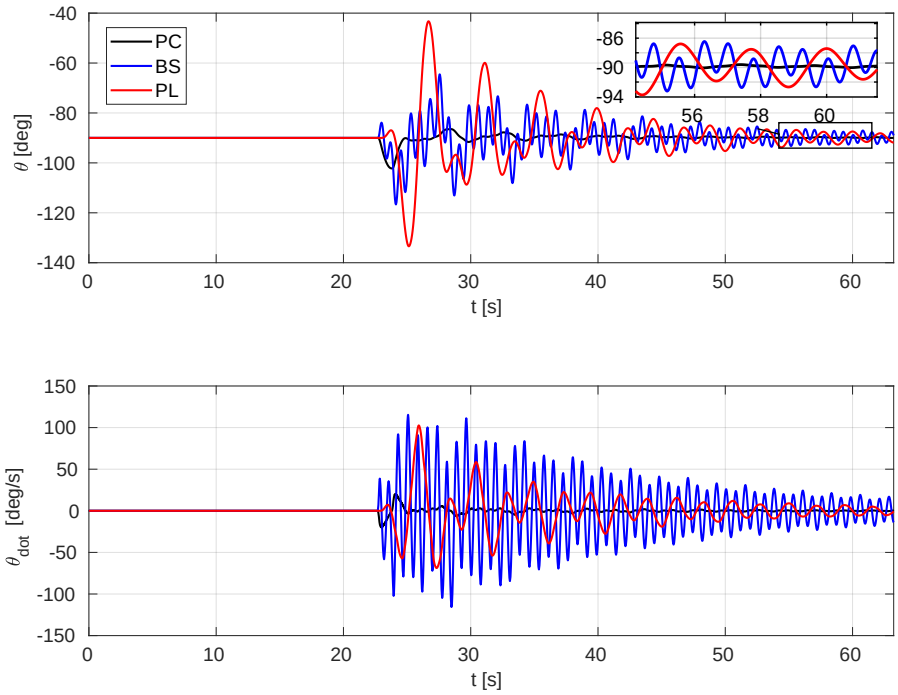

Figure 3. Effect of a sample wind gust on the attitude behaviour of the system.

fact, once the spacecraft baseline has been defined, its configuration can be adjusted by varying the lengths of the risers connecting the parachute with the backshell and the backshell with the payload, to achieve the desired dynamic response.

By running several gust response simulations with different lengths of both risers, it has been verified that these parameters have a marginal effect on the oscillatory behaviour of the parachute body. This was expected, because its attitude is dominated by the aerodynamic forces that grow as soon as its angle of attack moves with respect to the equilibrium condition. In addition to this, while the length of the riser between the parachute and the backshell $L_{\mathrm{r,pc\text{-}bs}}$ has a major influence on the backshell attitude behaviour, it only marginally influences the characteristics of the payload oscillations. The opposite happens for the riser between the backshell and the payload $L_{\mathrm{r,bs\text{-}pl}}$.

Figure 4 shows the oscillatory response of the backshell when the spacecraft is hit by a short 20 m/s horizontal gust, for different values of $L_{\mathrm{r,pc\text{-}bs}}$. The IC are those listed in Table 5 with the exception of the $z_{0,2}$ and $z_{0,3}$ initial position components. These depend indeed on the riser lengths that are varied in the figure, but can easily be determined by considering that the simulation starts with the vehicle oriented vertically and that the risers are not elongated at t_0. The same IC and gust are also used for Fig. 5. From this figure it is interesting to notice that, while the response for the cases of $L_{\mathrm{r,pc\text{-}bs}} = 0$ m and $L_{\mathrm{r,pc\text{-}bs}} = 10$ m is pretty much similar, in case of the intermediate value $L_{\mathrm{r,pc\text{-}bs}} = 5$ m the oscillations are damped much more efficiently and, still, the maximum backshell attitude angle variation does not go beyond 30°.

The influence of the backshell-payload riser length $L_{\mathrm{r,bs\text{-}pl}}$ on the oscillations of the payload body, that represents most of the mass of the MPF spacecraft, can easily be explained. Figure 5 confirms that, as expected, a shorter riser, that results in a lower moment of inertia for the lower section of the spacecraft (lower riser attached to the payload), causes the payload attitude angle oscillation amplitude to be larger at the impact of the gust, up to 40°, but also that these oscillations are damped faster in the remainder of the descent.

The stability of the backshell is fundamental, if during the descent the thrusters to be used for horizontal-position control are fixed with respect to it. In fact, these should always push as horizontally as possible. If the thrust direction oscillates, then the system loses efficiency. The condition $L_{\mathrm{r,pc\text{-}bs}} = 5$ m, even if it causes the impact of the gust to be a little bit more critical for the backshell, represents an optimum for the purpose of our guided system and will be used for studying the performance of the closed-loop system. With

Downloaded by TU DELFT on May 28, 2019 | http://arc.aiaa.org | DOI: 10.2514/6.2019-0665

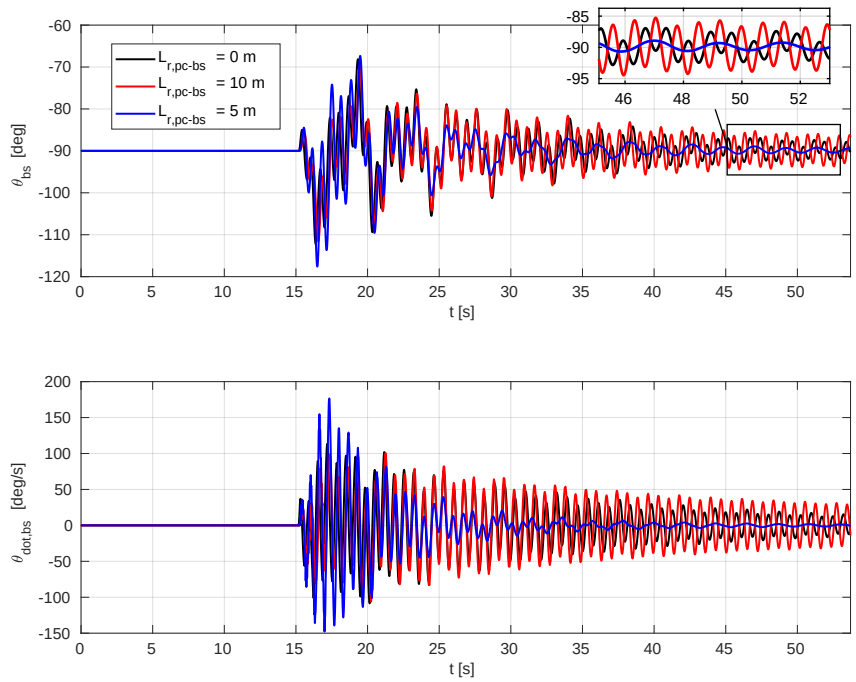

Figure 4. Effect of a sample wind gust on the attitude behaviour of the system for different parachute-backshell riser lengths.

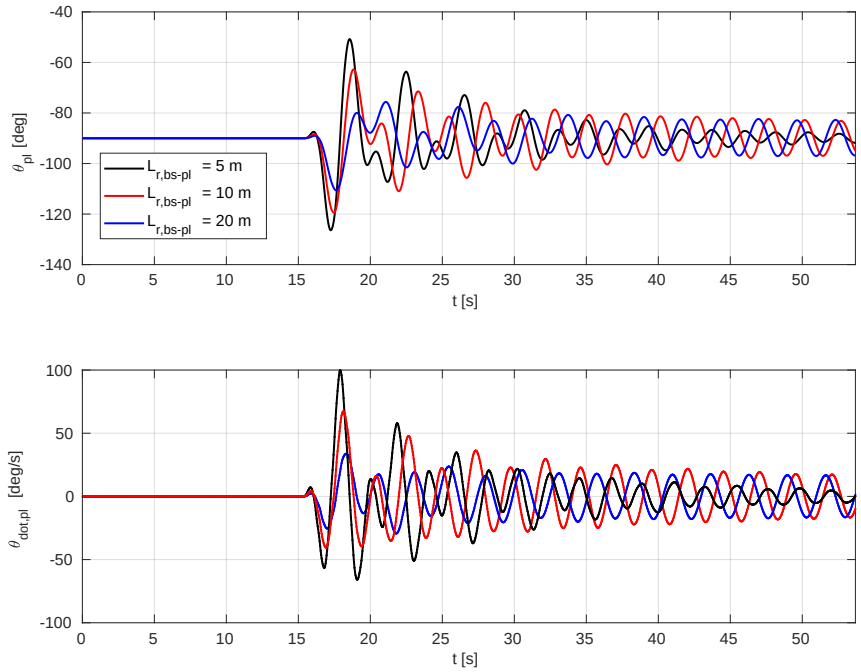

Figure 5. Effect of a sample wind gust on the attitude behaviour of the system for different backshell-payload riser lengths.

respect to the backshell-payload riser length, instead, a shorter riser, as already suggested earlier, results in a system that is more sensitive to external perturbations but damps the oscillations faster and is more responsive. The latter are desirable characteristics for the purpose of controlling the trajectory and thus this parameter will be kept equal to 5 m.

Table 6. Set of IC for the MPF new reference vehicle used for turbulence response and closed-loop system simulations.

Parameter	Value	Parameter	Value	Parameter	Value
γ_{10} [deg]	-90	γ_{20} [deg]	-90	γ_{30} [deg]	-90
θ_{10} [deg]	-90	θ_{20} [deg]	-90	θ_{30} [deg]	-90
$\dot{\theta}_{10}$ [deg/s]	0	$\dot{\theta}_{20}$ [deg/s]	0	$\dot{\theta}_{30}$ [deg/s]	0
V_{10} [m/s]	100	V_{20} [m/s]	100	V_{30} [m/s]	100
z_{10} [m]	6000	z_{20} [m]	5973.83	z_{30} [m]	5965.83
y_{10} [m]	0	y_{20} [m]	0	y_{30} [m]	0

When choosing the riser lengths, however, also impingement of the thrusters plumes with the parachute or payload has to be taken into account. For the original MPF spacecraft, equipped with backshell thrusters pushing downwards, the payload was at least at a distance of 20 m. In our case the thrusters push horizontally and we can accept a payload that is closer to the backshell, at more than 5 m. Also, since the spacecraft flies vertically, the plumes of the engines will extend upwards from the backshell to the parachute and this could represent a danger. However, the suspension lines, together with the parachute backshell riser, keep the canopy at a distance of around 25 m that is assumed to be adequate to avoid impingement.

The oscillatory behaviour of the attitude angles θ of the elements of the system was also tested while being exposed to turbulence. It was verified that the maximum frequency for the atmospheric turbulence on Mars, $\omega_t = 40.82$ Hz, is not an issue for the dynamics of the system. As the frequency decreases the effects of turbulence, especially on the parachute and backshell elements, become more significant. At 10 Hz these two bodies experience a resonance effect. The similarity of their attitude motion is due to the fact that they have comparable moments of inertia. However, the oscillation amplitude for the parachute is much smaller, because of the dominant contribution of the horizontal aerodynamic forces when its angle of attack increases. At these frequencies the motion of the payload is not yet significantly influenced because of the fact that it has a much larger moment of inertia. When reducing frequency even more, also the natural oscillation frequency of the payload body is matched at around 1-5 Hz. At this point, however, the turbulence is not an issue for the parachute and backshell elements any more. Below 1 Hz the influence of turbulence on the attitude behaviour of the system becomes progressively less important. At 0.1 Hz its effect on the spacecraft dynamics is comparable to that of a long lasting shallow gust and causes mainly oscillations in its horizontal velocity and, in turn, in the descent trajectory.

B. Closed-Loop System Performance

In the previous sections the characteristics of the spacecraft and of the guidance system for controlling its trajectory during the parachute descent have been defined. The only parameter for which a reference value has not been set yet is the maximum thrust $T_{\max}$ of the hydrazine backshell thrusters.

A larger $T_{\max}$ implies a larger maximum error that can be corrected and a better system responsiveness. On the other hand, however, the mass and volume of a hydrazine thruster is proportional to $T_{\max}$. In addition, a thrust push, similarly to a short wind gust, causes the attitude of the system to oscillate with an amplitude proportional to the intensity of the push, that in the worst case is $T_{\max}$. By running a number of tests with different sample errors between 100 and 500 m, that represent the order of magnitude of the wind drift error, it has been verified that the system responsiveness does not increase significantly with values of $T_{\max}$ larger than 500 N. A sudden push at $T_{\max} = 500$ N – estimated for a vehicle vertical speed of 100 m/s – also causes oscillations in θ, with a maximum amplitude of 35° (this worst case is for the payload whose oscillations have a larger amplitude than for the other elements). This is comparable to that due to an average wind gust. Finally, a 500 N hydrazine thruster weighs about 2 kg and is 45 cm long. These dimensions are considered to be acceptable for housing the thrusters in the backshell of the MPF spacecraft.

Now the reference configuration for the spacecraft is complete and we can use the available information to determine the performance that the parachute descent control system can achieve. Figure 6 shows how the system responds to initial errors of different magnitude. The initial condition for the trajectories depicted here are given in Table 6, except for the y position components that vary with the initial error. In general, the system always gets close to the equilibrium condition $y = 0,\ V_y = 0$, but, already for an initial error of

Downloaded by TU DELFT on May 28, 2019 | http://arc.aiaa.org | DOI: 10.2514/6.2019-0665

Downloaded by TU DELFT on May 28, 2019 | http://arc.aiaa.org | DOI: 10.2514/6.2019-0665

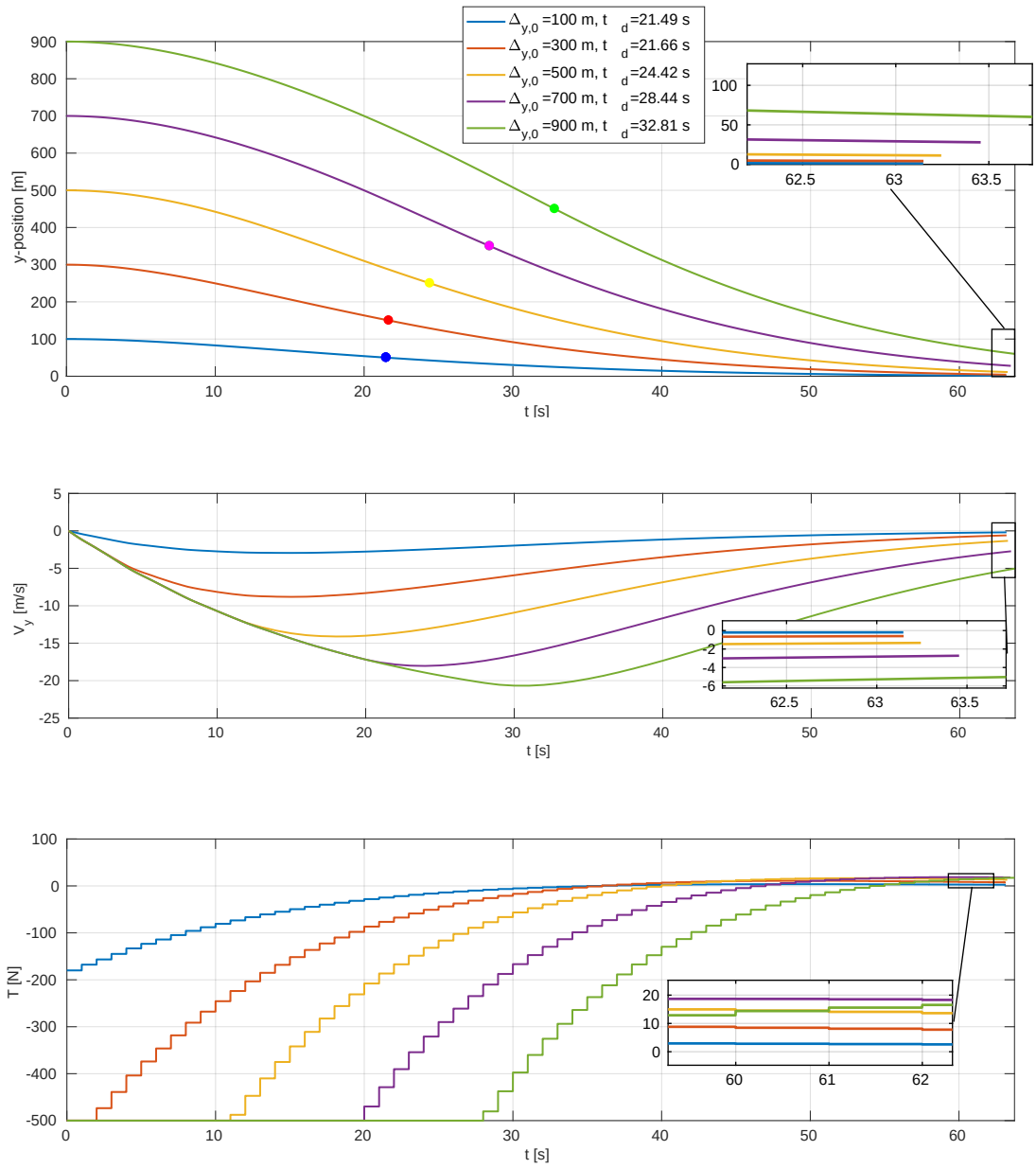

Figure 6. Response of the closed-loop system to different initial horizontal position errors.

900 m, the accuracy at target altitude is low. At this point the spacecraft is still 60 m away from its target and features a horizontal velocity just above 5 m/s. In this situation the system is clearly at its limit, this being confirmed by the fact that for half of the descent the thrusters are saturated. The situation improves if the error to correct is 700 or 500 m. However, even for a small initial error of 100 m, when the thrusters never saturate, a small residual error, in the order of 1 m and 0.1 m/s for the horizontal position and velocity, respectively, is present when the target altitude is reached. This is caused by the fact that when the position error is small, i.e., when the system is close to the target, then the proportional and derivative contributions determining the control signal have a comparable magnitude but opposite sign, so that the commanded thrust is about null and the spacecraft tends to fly almost vertically even if it has not yet reached the target. This behaviour can be changed by increasing the controller gain K_p or reducing K_d, or adding an integral component. This would result in a higher responsiveness at the cost of having a system that consumes more propellant and that oscillates around the equilibrium position, the latter also causing undesirable attitude

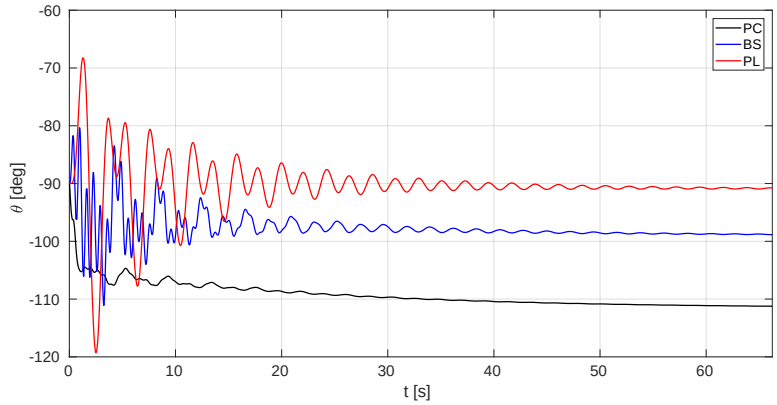

Figure 7. Effect of 26 m/s horizontal wind on the attitude behaviour of the closed-loop system.

Downloaded by TU DELFT on May 28, 2019 | http://arc.aiaa.org | DOI: 10.2514/6.2019-0665

oscillations of the non-rigid spacecraft. Finally, a larger initial position error causes the trajectory to be more curved and longer such that the total descent time will be larger as well.

Each of the trajectories depicted in Fig. 6 is characterised by a certain fuel consumption. Clearly, the maximum consumption of 7.1 kg of fuel is for $\Delta_{y,0} = 900$ m, while for correcting $\Delta_{y,0} = 100$ m the system needs 0.9 kg of hydrazine. Considering this, a tank containing 8 kg of fuel is assumed to be appropriate for ensuring control authority to handle different mission scenarios. If we assume that the backshell is equipped with 6 thrusters, then the whole guidance and control system for parachute descent, assuming that the computing hardware is the same already installed for guiding the entry and terminal descent phases, would have a mass of about 20 kg. This mass has not been taken into account in the calculations. However, this does not represent a problem because the MPF payload mass is much larger and 20 kg more would not dramatically affect the total descent time or trajectory. Conversely, if the thrusters and tank are installed in the backshell, then it would cause a non-negligible increase in its mass and moment of inertia, thus making its attitude less sensitive to external perturbations or thrust pushes.

While descending through the atmosphere of Mars the spacecraft can encounter constant winds. The thrust force generated by the backshell thrusters can be exploited to compensate the effect of wind up to a certain wind speed. It was verified that the thrust generated by the backshell engines can easily handle a horizontal wind with a speed up to 15 m/s. In fact, in these cases the system would be able to reach the target by simply pushing at $T_{\max}$ for a longer period. To achieve this, however, a more sophisticated control law taking the effective airspeed of the vehicle into account is needed. As the wind speed increases, the horizontal component of the aerodynamic force generated by the parachute increases as well, until at $V_w = 26$ m/s it almost balances with the thrust force. As Fig. 7 shows (initial conditions from Table 6, except $y_{1,0} = y_{2,0} = y_{3,0} = 500$ m), in this situation the parachute bends in the direction of the wind, opposite to the direction of the thrust, so that, assuming a wind with positive speed in the inertial frame I, its attitude angle increases. The equilibrium is reached when the horizontal component of the parachute drag equals the backshell thrust. This happens when $\theta_{\text{pc}} \approx -110°$. For wind speeds larger than 26 m/s the horizontal component of the parachute drag becomes dominant over the backshell thrust and the system cannot compensate for it any more, not even when pushing continuously at $T_{\max}$. By increasing $T_{\max}$, the maximum wind speed that can be compensated increases accordingly, but then the parachute has to bend even more with respect to the backshell to reach the equilibrium condition, and this represents an issue for impingement reasons. The fact that θ_{bs} does not stabilise exactly at -90° comes from the fact that the attitude of this element is influenced by both the forces generated by the parachute and payload that are transmitted through the risers. In the situation depicted in Fig. 7 the backshell is tilted in the same direction of the parachute, because the drag it generates is dominant over the payload weight.

The performance of the backshell thrust guidance system has been evaluated also in case the spacecraft is subjected to turbulence for the whole descent flight. In particular, the response has been tested using a turbulence frequency of 10 Hz that, as demonstrated earlier, is the most critical frequency for the attitude behaviour of the backshell and parachute, and 1 Hz, that is instead dangerous for the attitude oscillations of the payload body. The results of this analysis, however, have shown that the spacecraft trajectory, as

well as the overall guidance system consumption, are not significantly influenced by the presence of this perturbation.

VI. Conclusions

In the previous sections the dynamic stability properties of parachute-payload systems have been analysed. Also, it was defined how these vary in case the system is equipped with a guidance system based on backshell thrusters, whose performance in improving Mars landing accuracy has been evaluated. From this it emerged that the guided descent system, in absence of wind, is able to significantly reduce the horizontal position error. The position-velocity target accuracy, however, decreases for large initial horizontal position errors and is around 60 m and 5 m/s if the initial error is 900 m. This can be considered to be the limit of the system. The first disadvantage of using it is the fact that the use of thrust significantly affects the attitude of the system. It has been verified that a sudden push at $T_{\max} = 500$ N, which has been estimated to be an appropriate value with respect to the aim and constraints of the mission, causes dangerous oscillations of the body elements of the non-rigid spacecraft. However, a 20 m/s horizontal gust proved to be more critical for its attitude behaviour. This means that the response to gusts should still be used as primary test bed for the stability properties of a Mars descent spacecraft, even in case this is going to be equipped with a guidance system comparable to the one considered here.

The system can compensate a horizontal constant wind speed up to 26 m/s that represents an extreme condition. Also, the backshell thrust control system performance is only marginally affected by the presence of turbulences and gusts during the descent. The fuel needed for the descent depends on the conditions the spacecraft has to face. With a total amount of 8 kg of hydrazine the system can correct an horizontal position error of 900 m. This is assumed to be enough for most mission scenarios. This estimate, however, greatly varies in the real case due to navigation error that causes the fuel efficiency of the system to reduce dramatically. If the system includes also six thrusters, then the total extra mass of the guidance and control unit can be estimated around 20 kg. The additional vehicle mass due to the guidance and control hardware and fuel mass is a second disadvantage of using the descent guidance system.

References

[1]Wolf, A. A., Graves, C., Powell, R., and Johnson, W.,"Systems for pinpoint landing at Mars", *Advances in the Astronautical Sciences*, volume 119, no. SUPPL., 2005, pp. 2677-2696.

[2]Heinrich, H. G. and Haak, E. L.,"Stability and Drag of Parachutes with Varying Effective Porosity", Technical report, Air Force Flight Dynamics Laboratory, 1971.

[3]Helmut, G. H. and Lawrence Jr., W. R.,"Dynamic stability of a parachute point-mass load system", Report FDL-TDR-64-126, Department of Aeronautics and Engineering Mechanics, University of Minnesota, Minneapolis, Minnesota, 1965.

[4]Hume, R., "A Two dimensional Mathematical Model of a Parachute in Steady Descent", Technical Report 1260, Aeronautical Research Council, 1973.

[5]Abdulkadir, L., "*Stability of Multibody Systems for Mars Descent and Landing*", MSc Thesis, Delft University of Technology, 2011.

[6]Doherr, K.-F. and Schilling, H., "9DOF-simulation of rotating parachute systems", *11th Aerodynamic Decelerator Systems Technology Conference*, 1991.

[7]Fallon, E.,"Parachute dynamics and stability analysis of the Queen Match Recovery System", *11th Aerodynamic Decelerator Systems Technology Conference*, 1991.

[8]Ibrahim, S. and Engdahl, R.,"Parachute Dynamics and Stability Analysis" Technical report, System and Research Center Honeywell, Inc, 1974.

[9]Neustadt, M., Ericksen, R. E., Guiteras, J., and Larrivee, J.,"A parachute recovery system dynamic analysis", *Journal of Spacecraft and Rockets*, volume 4, no. 3, 1967, pp. 321-326.

[10]Mendeck, G. F. and Craig McGrew, L.,"Entry Guidance Design and Post-flight Performance for 2011 Mars Science Laboratory Mission", *Journal of Spacecraft and Rockets*, volume 51, no. 4, 2014, pp. 1094-1105.

[11]Cruz, J., Mineck, R., Keller, D., and Bobskill, M.,"Wind Tunnel Testing of Various Disk-Gap-Band Parachutes", *17th AIAA Aerodynamic Decelerator Systems Technology Conference and Seminar*, 2003.

[12]Prince, J., Desai, P., Queen, E., and Grover, M., "Mars Phoenix Entry, Descent, and Landing Simulation Design and Modeling Analysis", AIAA-2008-7507, AIAA/AAS Astrodynamics Specialist Conference and Exhibit, 2008.

[13]Kaas, D., Schofield, J., Michaels, T., Rafkin, S., Richardson, M., and Toigo, A., "Analysis of atmospheric mesoscale models for entry, descent, and landing", *Journal of Geophysical Research: Planets*, volume 10, 2003, pp.1–10.

[14]Haberle, R., Clancy, R., Forget, F., Smith, M., and Zurek, R., *The Atmosphere and Climate of Mars*, Cambridge University Press, 2017.

[15]Spencer, D. a. and Braun, R. D, "Mars Pathfinder atmospheric entry - Trajectory design and dispersion analysis", *Journal of Spacecraft and Rockets*, volume 33, no. 5, 1996, pp. 670–676.

Downloaded by TU DELFT on May 28, 2019 | http://arc.aiaa.org | DOI: 10.2514/6.2019-0665